International Journal of Pharmaceutics 701 (2026) 127103

Contents lists available at ScienceDirect

International Journal of Pharmaceutics

journal homepage: www.elsevier.com/locate/ijpharm

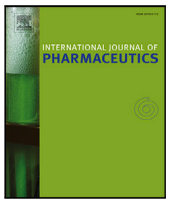

Effect of composition dependence in Flory–Huggins parameters on solid dispersion stability prediction

Martin Meere [a], Giuseppe Pontrelli [b], Sean McGinty [c,d,*]

[a] School of Mathematical and Statistical Sciences, University of Galway, Ireland
[b] Istituto per le Applicazioni del Calcolo — CNR, Via dei Taurini 19, Rome 00185, Italy
[c] Division of Biomedical Engineering, James Watt School of Engineering, University of Glasgow, Glasgow G12 8QQ, United Kingdom
[d] Glasgow Computational Engineering Centre, James Watt School of Engineering, University of Glasgow, Glasgow G12 8QQ, United Kingdom

ARTICLE INFO

Keywords:
Solid dispersion
Flory–Huggins
Phase diagram
Spinodal
Binodal
Cahn-Hilliard

ABSTRACT

Flory–Huggins models underpin phase diagram construction and stability analysis in a wide range of polymer–solute systems, including pharmaceutical solid dispersions, where phase diagrams are routinely used to guide formulation design and stability risk assessment during product development. In practice, the interaction parameter is commonly represented as a temperature-dependent function, $\chi = \chi(T)$, fitted to experimental data. However, multiple studies and experimental observations suggest that χ may depend on both temperature and composition (ϕ), that is, $\chi = \chi(\phi, T)$. Focusing on solid dispersions, here we develop and interrogate a novel composition-dependent Flory–Huggins mathematical framework and quantify the consequences of using $\chi(\phi, T)$ in place of $\chi(T)$ when predicting and interpreting phase behaviour. We derive the appropriate chemical potentials and stability conditions required for binodal and spinodal calculations when χ depends on both composition and temperature, and we present generalized criteria for the existence of both upper critical solution temperature (UCST) and lower critical solution temperature (LCST) behaviour. We construct phase diagrams for three solid dispersion systems based on independent experimental data taken from the literature and directly compare predictions obtained using $\chi = \chi(T)$ and $\chi = \chi(\phi, T)$ for each system. We demonstrate that allowing χ to depend on composition can lead not only to substantial quantitative differences, but also to qualitatively different phase behaviour. Finally, we illustrate the implications of these differing phase diagrams by developing a partial differential equation model that enables simulation of microstructural spatiotemporal evolution. The resulting simulations validate the predicted stability landscapes and reveal rich demixing morphologies, including bicontinuous networks and droplet formation.

1. Introduction

For a drug to exert its biological effect, it must be able to dissolve in order to reach the target tissues or cells (Siepmann et al., 2020). While around 60% of current commercially approved drugs are readily water soluble, it is estimated that around 90% of emerging drug candidates are poorly water soluble (Kim et al., 2021). Thus, the advancement of technologies that improve the bio-availability of these poorly water soluble drugs is urgently needed. One promising strategy to overcome this challenge is the design of solid dispersions (SDs) (Brough and Williams, 2013; Huang and Dai, 2014; Dhirendra et al., 2009), where the drug is mixed with one or more polymers in order to improve its solubility properties. A critical issue in the design of SDs is understanding the thermodynamic phase behaviour, since this has a significant impact on the stability, efficacy and manufacturability of the final pharmaceutical product. Drug in its amorphous state generally has a higher solubility and dissolution rate than in the crystalline form. However, the amorphous form is thermodynamically less stable, leading to a risk of recrystallization over time, which can reduce bioavailability and affect drug performance. Moreover, there is a tendency for amorphous drug to crystallize during storage or under different environmental conditions (e.g., temperature, humidity). Phase separation, where the drug and polymer segregate into distinct domains, is a further challenge, and can result in uneven drug distribution, reduced drug release rates and instability. There are also implications in terms of drug loading, since higher drug loading can lead to supersaturation, increasing the likelihood of crystallization and phase separation. Thus, balancing the drug load with the stability of the dispersion is a key challenge in the formulation of SDs.

* Corresponding author.
E-mail address: sean.mcginty@glasgow.ac.uk (S. McGinty).

https://doi.org/10.1016/j.ijpharm.2026.127103
Received 5 May 2026; Received in revised form 15 June 2026; Accepted 15 June 2026
Available online 20 June 2026

An essential tool for understanding and predicting the phase behaviour of SDs is the construction of phase diagrams. A phase diagram is a graphical representation that shows the relationship between different phases of a system composed of a drug and polymer as a function of temperature and composition. From the phase diagram, it is possible to understand how different phases coexist and transition under various conditions. Key features of the phase diagram are the binodal curve and the spinodal curve. These curves describe the boundaries of phase separation and enable prediction of the conditions under which a homogeneous mixture may separate into distinct phases. Specifically, the binodal curve represents the boundary in a phase diagram that separates the single-phase region (where the drug and polymer are fully miscible) from the two-phase region (where phase separation occurs). The spinodal curve is located within the two-phase region and represents the boundary inside which spontaneous phase separation occurs. Between the binodal and spinodal curves lies a metastable region. In this region, the mixture is not fully stable, but may phase separate under certain conditions.

Phase diagrams are constructed with the aid of thermodynamic models. The most widely used thermodynamic model in this context is the Flory–Huggins (FH) model (Flory, 1942; Huggins, 1941; Hiemenz and Lodge, 2007) for polymer solutions. In the context of a drug/polymer binary system, FH theory enables the calculation of the change in Gibbs free energy (ΔG_{mix}) per mole associated with mixing:

$$\frac{\Delta G_{mix}}{RT} = X_d \ln(\phi_d) + X_p \ln(\phi_p) + \chi_{dp} X_d \phi_p, \tag{1}$$

where R is the gas constant, T is the temperature, $X_d, X_p = 1 - X_d$ are the mole fractions of the drug and polymer, respectively, and ϕ_d, ϕ_p are the volume fractions of the drug and polymer, respectively, related via

$$\phi_d = \frac{X_d}{X_d + mX_p}, \quad \phi_p = \frac{mX_p}{X_d + mX_p}, \tag{2}$$

where

$$m = \frac{V_p}{V_d}, \tag{3}$$

and where V_p, V_d are the molar volumes of the polymer and drug, respectively. Here $m > 1$ usually since polymer molecules are typically larger than drug molecules. The quantity χ_{dp} is referred to as the FH interaction parameter which may, in general, be both temperature and composition-dependent (Koningsveld et al., 1993; Koningsveld, 1994; Tian et al., 2013a). In the context of drug-polymer interactions, this parameter has historically been estimated as either a constant value or varying in proportion to the inverse of temperature T (Potter et al., 2018):

$$\chi_{dp}(T) = A + \frac{B}{T}, \tag{4}$$

where A, B (K) are constants. This parameter needs to be determined experimentally, and there are various methods of doing so. However, FH interaction parameters are typically obtained over a small temperature and composition range, primarily due to limitations in obtaining the necessary experimental data. One of the most common methods is melting point depression (Taylor, 2018; Rask et al., 2018; Altamimi and Neau, 2016) which usually requires high temperatures. Moreover, this method is associated with lower accuracy at low drug fractions. Thus, χ_{dp} is often measured at high temperature and higher drug loadings, which has potential implications on accuracy when extrapolating to lower temperatures and low drug loadings.

In an attempt to address this issue, in recent years there has been increasing interest in the specific form of the FH interaction parameter (Potter et al., 2018; Klueppelberg et al., 2023; Tian et al., 2019; Wolf, 2003). In particular, several studies have shown that an additional composition dependence of the FH interaction parameter χ_{dp} yields better agreement with experimental data than (4). For example, Potter et al. (2018) employed a highly-sensitive differential scanning calorimetry (DSC) technique and found that the linear relationship in (4) broke down when considering smaller amounts of drug. They demonstrated that a quadratic dependence of χ_{dp} on composition of the form:

$$\chi_{dp}(\phi_d, T) = A + \frac{B}{T} + C\phi_d + E\phi_d^2, \tag{5}$$

with C, E constants, yielded an improved fit to experimental data. More recently, Klueppelberg et al. (2023) demonstrated that a similar quadratic relationship well-described experimental measurements of χ_{dp} across 9 different drug-polymer combinations. Seeking to determine FH interaction parameters over a wider range of temperatures and drug loadings (specifically at lower temperatures and lower drug loadings), Tian et al. (2019) estimated χ_{dp} by combining data from two different experimental techniques. Specifically, they combined data obtained at high temperatures and high drug loadings (using the melting point depression method) with data obtained at lower temperatures and lower drug loadings using an amorphous drug-amorphous polymer phase separation (AAPS) approach. Briefly, the AAPS approach involved consideration of a ternary system via addition of water to the drug-polymer system under study, to accelerate the phase separation at lower temperatures, coupled with knowledge of the FH interaction parameters for the respective binary systems, obtained using more standard techniques.

Despite the increasing experimental interest in considering χ_{dp} a function of both temperature and composition, we are not aware of any theoretical studies which calculate the phase behaviour assuming a form of χ_{dp} that depends on drug composition. Thus the key novelty of this paper is the derivation and calculation of the phase diagram (spinodal curve, binodal curve and critical points) for several distinct drug-polymer systems, using expressions for $\chi_{dp}(\phi_d, T)$ derived from experiments in the literature. This enables us to (i) derive new criteria for determining whether a critical point is a lower critical solution temperature (LCST) or upper critical solution temperature (UCST) when $\chi_{dp}(\phi_d, T)$ and (ii) for the first time, directly compare, for $\chi_{dp}(T)$ and $\chi_{dp}(\phi_d, T)$, predictions of regions in the phase diagram where the system is stable/unstable/metastable. For a particular drug-polymer system, we validate the predictions from our phase diagram by simulating the spatiotemporal evolution of the solid dispersion using a partial differential equation formulation derived from consideration of the chemical potential. We conclude by discussing the potential implications on predictions of phase behaviour when extending FH interactions parameters beyond $1/T$ relationships and over a wider range of compositions and temperatures.

2. Theoretical formulation

2.1. Construction of the phase diagram for binary mixtures

The construction of binary phase diagrams has been well described elsewhere (see, for example, Hiemenz and Lodge (2007) or Tompa (1956)) and so our descriptions here will be brief, and will focus on the novel features of the calculations due to the composition dependence in the interaction parameter.

2.1.1. Stability of the binary mixture

We analyse the stability of the binary mixture using the Gibbs free energy of mixing given by (1). We write

$$\frac{\Delta G_{mix}(X_d, T)}{RT} = X_d \ln(\phi_d(X_d)) + (1 - X_d)\ln(\phi_p(X_d)) + \chi_{dp}(\phi_d(X_d), T) X_d \phi_p(X_d), \tag{6}$$

where (recalling Eqs. (2))

$$\phi_d(X_d) = \frac{X_d}{m - (m-1)X_d}, \quad \phi_p(X_d) = \frac{m(1 - X_d)}{m - (m-1)X_d}. \tag{7}$$

Using (6) and (7), straightforward calculation gives

$$\frac{\partial^2}{\partial X_d^2}\left(\frac{\Delta G_{mix}(X_d,T)}{RT}\right) = \frac{(1+(m-1)\phi_d)^3}{m\phi_d(1-\phi_d)}\Big[1+(1/m-1)\,\phi_d + \phi_d(1-\phi_d)\{-2\chi_{dp}(\phi_d,T)+2(1-2\phi_d)\chi'_{dp}(\phi_d,T) + \phi_d(1-\phi_d)\chi''_{dp}(\phi_d,T)\}\Big], \tag{8}$$

where $\chi'_{dp}(\phi_d,T) = \left(\frac{\partial \chi_{dp}(\phi_d,T)}{\partial \phi_d}\right)_T$. The binary mixture is unstable for a composition X_d if (Hiemenz and Lodge, 2007)

$$\frac{\partial^2 \Delta G_{mix}(X_d,T)}{\partial X_d^2} < 0.$$

2.1.2. The spinodal curve

For a given temperature T, the *spinodal points* are calculated by solving (see, for example, Chapter 7 of Hiemenz and Lodge (2007))

$$\frac{\partial^2 \Delta G_{mix}(X_d,T)}{\partial X_d^2} = 0, \tag{9}$$

for X_d where ΔG_{mix} is given by (6), (7). Repeating this calculation for different temperatures T yields the spinodal curve in (X_d,T) space, and this is easily translated into a curve in (ϕ_d,T) space.

From (8) and (9), the spinodal points are obtained by solving

$$0 = 1+\left(\frac{1}{m}-1\right)\phi_d + \phi_d(1-\phi_d)\Big[-2\chi_{dp}(\phi_d,T)+2(1-2\phi_d)\chi'_{dp}(\phi_d,T) + \phi_d(1-\phi_d)\chi''_{dp}(\phi_d,T)\Big], \tag{10}$$

for ϕ_d. Clearly the solutions to (10) will depend on the character of $\chi_{dp}(\phi_d,T)$. For the $\chi_{dp}(\phi_d,T)$ given by (5), Eq. (10) is a quartic for ϕ_d.

2.1.3. The binodal curve

For a given temperature T, two points on the *binodal curve* in (ϕ_d,T) space are denoted by (ϕ_{dL},T) and (ϕ_{dR},T) with $\phi_{dL} \neq \phi_{dR}$. The values for ϕ_{dL}, ϕ_{dR} are found by simultaneously solving the pair of equations for the bulk chemical potentials μ_d^b and μ_p^b (see Hiemenz and Lodge (2007))

$$\mu_d^b(\phi_{dL},T) = \mu_d^b(\phi_{dR},T), \quad \mu_p^b(\phi_{dL},T) = \mu_p^b(\phi_{dR},T). \tag{11}$$

It is noteworthy that the expressions for μ_d^b and μ_p^b here differ from those of earlier papers as a result of the non-standard dependence of χ on composition and temperature, rather than on temperature only (Meere et al., 2019). Thus, the chemical potentials need to be re-derived here. We have

$$\Delta\mu_d^b = \mu_d^b - \mu_d^0 = \left(\frac{\partial \Delta G_{mix}}{\partial X_d}\right)_{T,X_p}, \tag{12}$$

where μ_d^0 is the chemical potential of the drug in its pure form, and where the derivative here is taken with respect to X_d holding X_p and the temperature T fixed. Using (1), Eq. (12) leads to

$$\mu_d^b = \mu_d^0 + RT\left(\ln(\phi_d)+\left(1-\frac{1}{m}\right)\phi_p+\chi_{dp}(\phi_d,T)\phi_p^2+\chi'_{dp}(\phi_d,T)\phi_d\phi_p^2\right), \tag{13}$$

where the volume fractions ϕ_d, ϕ_p are given by (2). From (5), it is clear that

$$\chi'_{dp}(\phi_d,T) = C + 2E\phi_d. \tag{14}$$

The term involving χ'_{dp} in (13) is noteworthy here since it does not feature in the standard FH expressions for an interaction parameter that depends on temperature only. An expression for the polymer chemical potential is obtained by differentiating ΔG_{mix} with respect to X_p, and this leads to

$$\mu_p^b = \mu_p^0 + RT\left(\ln(\phi_p)+(1-m)\,\phi_d + m\chi_{dp}(\phi_d,T)\phi_d^2 - m\chi'_{dp}(\phi_d,T)\phi_d^2\phi_p\right). \tag{15}$$

2.1.4. Critical points

The final feature of phase diagrams left to describe are *critical points*. These are points (X_c,T_c) in (X_d,T) space for which the spinodal curve has a stationary point (see Appendix B), and they correspond to locations where the spinodal and binodal points merge. Since critical points (X_c,T_c) lie on the spinodal curve, we have

$$\frac{\partial^2 \Delta G_{mix}}{\partial X_d^2}(X_c,T_c) = 0. \tag{16}$$

However (16) is insufficient to determine (X_c,T_c) since there are two unknowns. A second equation is provided by (see Appendix B)

$$\frac{\partial^3 \Delta G_{mix}}{\partial X_d^3}(X_c,T_c) = 0. \tag{17}$$

Solving (16) and (17) simultaneously for (X_c,T_c) determines the critical points.

A critical point can be either a Lower Critical Solution Temperature (LCST) or an Upper Critical Solution Temperature (UCST). If a critical point is a LCST (UCST), then the mixture is stably miscible for all compositions and for all temperatures $T < T_c$ ($T > T_c$). In Appendix B, we establish the following criteria for determining whether a critical point is a LCST or an UCST: if

$$\tau = \frac{1}{T_c}\left(\frac{\frac{\partial^4 \Delta G_{mix}}{\partial X_d^4}}{\frac{\partial^3 \Delta G_{mix}}{\partial X_d^2 \partial T}}\right)_{(X_c,T_c)} < 0 \quad \Rightarrow \quad (X_c,T_c) \text{ is a LCST,} \tag{18}$$

and if

$$\tau = \frac{1}{T_c}\left(\frac{\frac{\partial^4 \Delta G_{mix}}{\partial X_d^4}}{\frac{\partial^3 \Delta G_{mix}}{\partial X_d^2 \partial T}}\right)_{(X_c,T_c)} > 0 \quad \Rightarrow \quad (X_c,T_c) \text{ is an UCST.} \tag{19}$$

For the particular case of FH theory where the interaction parameter depends on the temperature only, so that $\chi_{dp} = \chi_{dp}(T)$, these conditions reduce to (omitting details of the calculation)

$$\frac{1}{T_c}\frac{\chi_{dp}(T_c)}{\frac{\partial \chi_{dp}}{\partial T}(T_c)} > 0 \quad \Rightarrow \quad (X_c,T_c) \text{ is a LCST,} \tag{20}$$

and

$$\frac{1}{T_c}\frac{\chi_{dp}(T_c)}{\frac{\partial \chi_{dp}}{\partial T}(T_c)} < 0 \quad \Rightarrow \quad (X_c,T_c) \text{ is an UCST.} \tag{21}$$

2.2. Modelling the evolution of the solid dispersions

In an earlier paper by Meere et al. (2019), a partial differential equations model was developed to describe the evolution of a solid dispersion mixture. The same overall model structure will be employed in the current study, although some details will differ as a result of the consideration of the composition dependence of χ_{dp}. We will give a brief description of the model here, and refer the interested reader to Meere et al. (2019) for more details.

The spatio-temporal formulation for the FH model involving the chemical potential μ_d and self-diffusion coefficient (D_d) for the drug is given by (see Meere et al. (2019)):

$$\frac{\partial X_d}{\partial t} = \nabla\cdot\left(D_d X_d \nabla\psi\right), \tag{22}$$

where

$$\psi = \frac{\mu_d - \mu_d^0}{RT} = \ln(a_d) - \delta_d^2\nabla^2 X_d. \tag{23}$$

As discussed in Meere et al. (2019), $a_d = \gamma_d X_d$ refers to the drug activity, with γ_d referring to the activity coefficient, and the term involving $\delta_d^2 > 0$ energetically penalizes the formation of sharp phase boundaries.

One may derive the following expression for ψ by consideration of (23) with (13):

$$\psi = \ln\left(\frac{X_d}{m-(m-1)X_d}\right) + \frac{(m-1)(1-X_d)}{m-(m-1)X_d} + \chi_{dp}(\phi_d,T)m^2\left(\frac{1-X_d}{m-(m-1)X_d}\right)^2 + \chi'_{dp}(\phi_d,T)\frac{m^2X_d(1-X_d)^2}{(m-(m-1)X_d)^3} - \delta_d^2\nabla^2X_d. \quad (24)$$

Eqs. (22)–(24) retain the classical Cahn–Hilliard structure; however, the assumption $\chi_{dp} = \chi_{dp}(\phi_d, T)$ gives rise to additional χ'_{dp} contributions in the chemical potential compared with conventional formulations based on $\chi_{dp} = \chi_{dp}(T)$. It is also worth noting that the mobility is proportional to the drug molar fraction here. While composition-dependent mobilities are common in Cahn–Hilliard models, this asymmetric choice differs from standard previous forms and is derived from a multicomponent diffusion approach (see Meere et al. (2019)).

We suppose that the solid dispersion occupies a two-dimensional region Ω. The governing equation for the drug concentration in Ω may be written in the conservation form

$$\frac{\partial X_d}{\partial t} + \nabla\cdot\mathbf{J}_d = 0,$$

where the drug flux $\mathbf{J}_d$ is given by

$$\mathbf{J}_d = -D_dX_d\nabla\psi. \quad (25)$$

We need to supplement the governing equation in Ω with boundary conditions on its boundary $\partial\Omega$, and we choose these here to be

$$\mathbf{J}_d\cdot\mathbf{n} = 0, \qquad \nabla X_d\cdot\mathbf{n} = 0 \qquad \text{on} \qquad \partial\Omega. \quad (26)$$

The first of these conditions $\mathbf{J}_d\cdot\mathbf{n} = 0$ implies that the drug cannot penetrate the boundary of the domain. The other condition $\nabla X_d\cdot\mathbf{n} = 0$ is the natural boundary condition for the variational formulation of the problem, and it implies that the interfaces between the polymer rich and the drug rich domains meet the boundary at right angles.

Finally, to obtain a well-posed problem, we need to impose an initial condition and we choose this here to take the form

$$X_d(x,y,t=0) = X_d^0(x,y) \qquad \text{for} \qquad (x,y)\in\Omega, \quad (27)$$

where $X_d^0(x,y)$ is a given function.

Gathering together the governing equation, the boundary conditions and the initial condition, we obtain the following well-posed initial boundary value problem:

$$\begin{aligned} &\frac{\partial X_d}{\partial t} = \nabla\cdot\left(D_dX_d\nabla\psi\right) \qquad \text{in} \qquad \Omega,\\ &\nabla X_d\cdot\mathbf{n} = 0, \qquad \mathbf{J}_d\cdot\mathbf{n} = 0 \qquad \text{on} \qquad \partial\Omega,\\ &X_d(x,y,t=0) = X_d^0(x,y) \qquad \text{for} \qquad (x,y)\in\Omega. \end{aligned} \quad (28)$$

2.3. Numerical methods

2.3.1. Calculation of the phase diagrams

To calculate the spinodal, binodal and critical points for this study, we solved Eqs. (10), (11) and (16)–(17), respectively, using the mathematical software package MAPLE. In the case of the spinodal equation, repeatedly solving (10) using the `fsolve` command for different temperatures T generates the spinodal curve in (ϕ_d, T) space. The equations determining the binodal points (11) were also solved using the `fsolve` command, and the trivial solution $\phi_{dL} = \phi_{dR}$ was avoided by supplying the solver with initial guesses for ϕ_{dL} and ϕ_{dR} based on the corresponding spinodal points for the given temperature T. Repeating this calculation for different values of the temperature T generates the binodal curve in (ϕ_d, T) space.

2.3.2. Solution of the initial boundary value problem for solid dispersion evolution

We now describe the numerical method for solving the initial boundary value problem (28). The numerical integration was carried out using the finite element package COMSOL Multiphysics (COMSOL AB, 2024). For the purposes of the numerical calculations, we took the integration domain to be the square region

$$\Omega = \{(x,y)|\ 0<x<L, 0<y<L\}.$$

We choose to perform two-dimensional calculations here because they are computationally cheaper than three-dimensional calculations, while still being sufficient to capture the key qualitative spatial behaviours of interest, including spinodal decomposition, coarsening, and droplet formation.

For the numerical calculations here, we chose to use non-dimensional variables for space and time by defining

$$x^* = \frac{x}{L}, \quad y^* = \frac{y}{L}, \quad t^* = \frac{t}{\left(L^2/D_d\right)},$$

so that the non-dimensional spatial domain becomes $\Omega^* = \{(x^*,y^*)|\ 0<x^*<1, 0<y^*<1\}$, and the nondimensional governing partial differential equation is (note that X_d and ψ here are already dimensionless)

$$\frac{\partial X_d}{\partial t^*} = \nabla^*\cdot\left(X_d\nabla^*\psi\right) \qquad \text{in} \qquad \Omega^*,$$

with $\nabla^* = (\partial/\partial x^*, \partial/\partial y^*)$. The advantage of this approach is that values for D_d are not required to implement the calculations, and the reliable estimation of D_d at storage-relevant conditions is inherently difficult since these values can be sensitive to factors such as temperature and relative humidity (see Rumondor et al. (2009)). The main drawback of this approach of course is that it does not provide information about the actual timescale of system evolution. Nevertheless, the main focus here is on tracking the spatial evolution of the system (particularly for unstable regimes), and our calculations will capture this behaviour.

A mesh sensitivity analysis was performed to investigate the influence of the size of the mesh on the results. The solution was assumed to be mesh independent when there was less than 1% difference in the mole fraction of drug between successive refinements. The final mesh used in the simulations was triangular and consisted of 7553 vertices and 14 796 triangles. The numerical solutions all conserved the total mass of drug in the system to within 1%.

The present work focuses on the thermodynamic implications of adopting $\chi = \chi(\phi, T)$ rather than on the development of specialized numerical algorithms. Accordingly, the governing equations were solved using the finite-element framework available in COMSOL Multiphysics (COMSOL AB, 2024). We note that positivity-preserving and energy-stable discretizations for Cahn–Hilliard-type equations with logarithmic free energies have attracted considerable recent attention (see Chen et al. (2019)); however, analysis of such properties for the numerical implementation employed here is beyond the scope of the present study.

2.3.3. Parameter values

To demonstrate the utility of our theoretical framework in calculating and comparing phase diagrams, we consider three distinct drug-polymer systems for which FH interaction parameters have been proposed in both the temperature-dependent form $\chi_{dp} = \chi_{dp}(T)$ and the temperature plus composition-dependent form $\chi_{dp} = \chi_{dp}(\phi_d, T)$. These systems are Felodipine (FD) - PVPK15 (Tian et al., 2019, 2013b), Itraconazole (ITZ)-Soluplus (SOL) (Potter et al., 2018), and ITZ-HPMCP (Potter et al., 2018). A summary of the forms for the FH interaction parameters is given in Table 1. The experimental studies used to determine these forms are briefly described in Table 2.

The molar volume for FD is $V_d = 300.19\ \text{cm}^3/\text{mol}$ (see Tian et al. (2013a)). In Tian et al. (2019), the molecular mass of PVPK15 ranged from 7000 g/mole to 11 000 g/mole. Here we take the molecular mass of the polymer to be at the midpoint of this range, $M_p = 9000$ g/mole.

Table 1
Summary of FH interaction parameters for the three systems under consideration in this study. The constants A, B, C and E refer to the formula (5).

Form of χ_{dp}	A	B	C	E	Reference
$\chi_{\text{ITZ-SOL}}(T)$	−36.3	15 029	–	–	Potter et al. (2018)
$\chi_{\text{ITZ-SOL}}(\phi_{\text{ITZ}}, T)$	−22.0	8433.75	10.4	−14.4	Potter et al. (2018)
$\chi_{\text{ITZ-HPMC}}(T)$	−58.2	23 599	–	–	Potter et al. (2018)
$\chi_{\text{ITZ-HPMC}}(\phi_{\text{ITZ}}, T)$	−292.2	111 776	93.13	−71.1	Potter et al. (2018)
$\chi_{\text{FD-PVPK15}}(T)$	−10.383	3679.2	–	–	Tian et al. (2013b)
$\chi_{\text{FD-PVPK15}}(\phi_{\text{FD}}, T)$	1.72	−852	5.17	−7.85	Tian et al. (2019)

Table 2
The experimental studies that determined the FH interaction parameters $\chi_{\text{DRUG-POLYMER}}$ for the systems considered in this study.

Figure	Study	Experimental Methods Used To Determine $\chi_{\text{DRUG-POLYMER}}$
Fig. 1(c), two terms FD-PVPK15	Tian et al. (2013b)	Melting point depression experiments were conducted for various drug loadings in FD-PVPK15 dispersions. Estimates for $\chi_{\text{FD-PVPK15}}(T_m)$ for various melting temperatures T_m were obtained using the experimental data in conjunction with the formula (in familiar notation; see Tian et al. (2013a)) $$\ln\phi_d + \left(1 - \frac{1}{m}\right)\phi_p + \chi_{\text{FD-PVPK15}}(T_m)\phi_P^2 = -\frac{\Delta H_f}{R}\left(\frac{1}{T_m} - \frac{1}{T_{m0}}\right).$$ The estimates for $\chi_{\text{FD-PVPK15}}(T)$ were then fitted to the form $$\chi_{\text{FD-PVPK15}}(T) = A + B/T$$ to give $A = -10.383$ and $B = 3679.2$.
Fig. 1(c), four terms FD-PVPK15	Tian et al. (2019)	For high temperatures, the data for $\chi_{\text{FD-PVPK15}}$ found in the paper (Tian et al., 2013b) were used. For lower temperatures, a more intricate approach was adopted to estimate $\chi_{\text{FD-PVPK15}}$. Water was introduced to the drug-polymer system as an accelerant for phase separation at lower temperatures. Binodal points for this ternary system were estimated experimentally using differential scanning calorimetry to determine the temperature at which the system switched from having one T_g (single phase) to two T_gs (two phases). With the experimental binodal points in hand, estimates for $\chi_{\text{FD-PVPK15}}$ were then obtained by numerically solving the three binodal equations given by ternary FH theory (we are omitting some details here for brevity). The data for $\chi_{\text{FD-PVPK15}}$ were then fitted to the form $$\chi_{\text{FD-PVPK15}}(\phi_d, T) = A + B/T + C\phi_d + E\phi_d^2$$ to give $A = 1.72$, $B = -852$, $C = 5.17$, $E = -7.85$.
Fig. 1(a), ITZ-SOL Fig. 1(b), ITZ-HPMCP	Potter et al. (2018)	Drug solubilities in polymers were determined using the *residual crystallinity method*. This method involved using differential scanning calorimetery to determine the critical annealing temperature below which drug begins to crystallize out of the polymer for a given drug fraction (the solubility temperature T_s). Estimates for $\chi_{\text{DRUG-POLY}}(\phi_d, T_s)$ for various drug fractions ϕ_d and temperatures T_s were obtained using the experimental data in conjunction with the formula $$\ln\phi_d + \left(1 - \frac{1}{m}\right)\phi_p + \chi_{\text{DRUG-POLYMER}}(\phi_d, T_s)\phi_P^2 = -\frac{\Delta H_f}{R}\left(\frac{1}{T_s} - \frac{1}{T_{m0}}\right).$$ This equation is structurally identical to the melting point depression formula given above, except that here T_s refers to a solubility temperature and not a melting temperature. The data for $\chi_{\text{DRUG-POLYMER}}(\phi_d, T)$ were then fitted to the form (four-term fitting) $$\chi_{\text{DRUG-POLYMER}}(\phi_d, T) = A + B/T + C\phi_d + E\phi_d^2$$ to give $A = -22.0$, $B = 8433.75$, $C = 10.4$, $E = -14.4$ for the ITZ-SOL system, and $A = -292.2$, $B = 111\,776$, $C = 93.13$, $E = -71.1$ for the ITZ-HPMCP system. A two-term fitting $\chi_{\text{DRUG-POLYMER}}(T) = A + B/T$ was also implemented.

The mass density of the polymer is $\rho_p = 1.2$ g/cm^3, so that its molar volume is given by

$$V_p = \frac{M_p}{\rho_p} = \frac{9000}{1.2} = 7500 \ \text{cm}^3/\text{mole},$$

and then

$$m_{\text{FD-PVPK15}} = \frac{V_p}{V_d} = \frac{7500}{300.19} \approx 24.98.$$

Similar calculations for the other two systems gives (see Table 3)

$$m_{\text{ITZ-SOL}} \approx 196.28, \quad m_{\text{ITZ-HPMC}} \approx 52.88.$$

When plotting phase diagrams, we will find it convenient to use the weight fraction of the drug (W_d), and this can be calculated using the volume fractions as follows

$$W_d = \frac{\rho_d\phi_d}{\rho_d\phi_d + \rho_p\phi_p},$$

where ρ_d, ρ_p are the mass densities of the drug and polymer, respectively.

For the FD-PVPK15 system, we further simulate the spatio-temporal evolution of the solid dispersion, which requires some further parameter inputs. The thickness of the interfacial regions is dictated by the parameter δ_d, and here we chose the value $\delta_d = L/50 = 4 \times 10^{-5}$ m. We illustrate how the initial conditions were specified by considering a particular case. We take the case where the initial volume fraction of drug is 50%, which corresponds to an initial molar drug fraction of $X_d = 0.9615$. More precisely, we chose the initial molar fraction of drug to be a small random perturbation about this level given by

$$X_d(x^*, y^*, t = 0) = 0.9615(1 + rnd(x^*, y^*))$$

where $rnd(x^*, y^*)$ is a normally distributed random function with a mean value of zero and a standard deviation of 10^{-5}.

3. Results and discussion

3.1. Phase diagram for the FD-PVPK15, ITZ-SOL and ITZ-HPMCP systems

We now calculate the phase diagram for the three systems listed in Section 2.3, and using the methods described there. The resulting

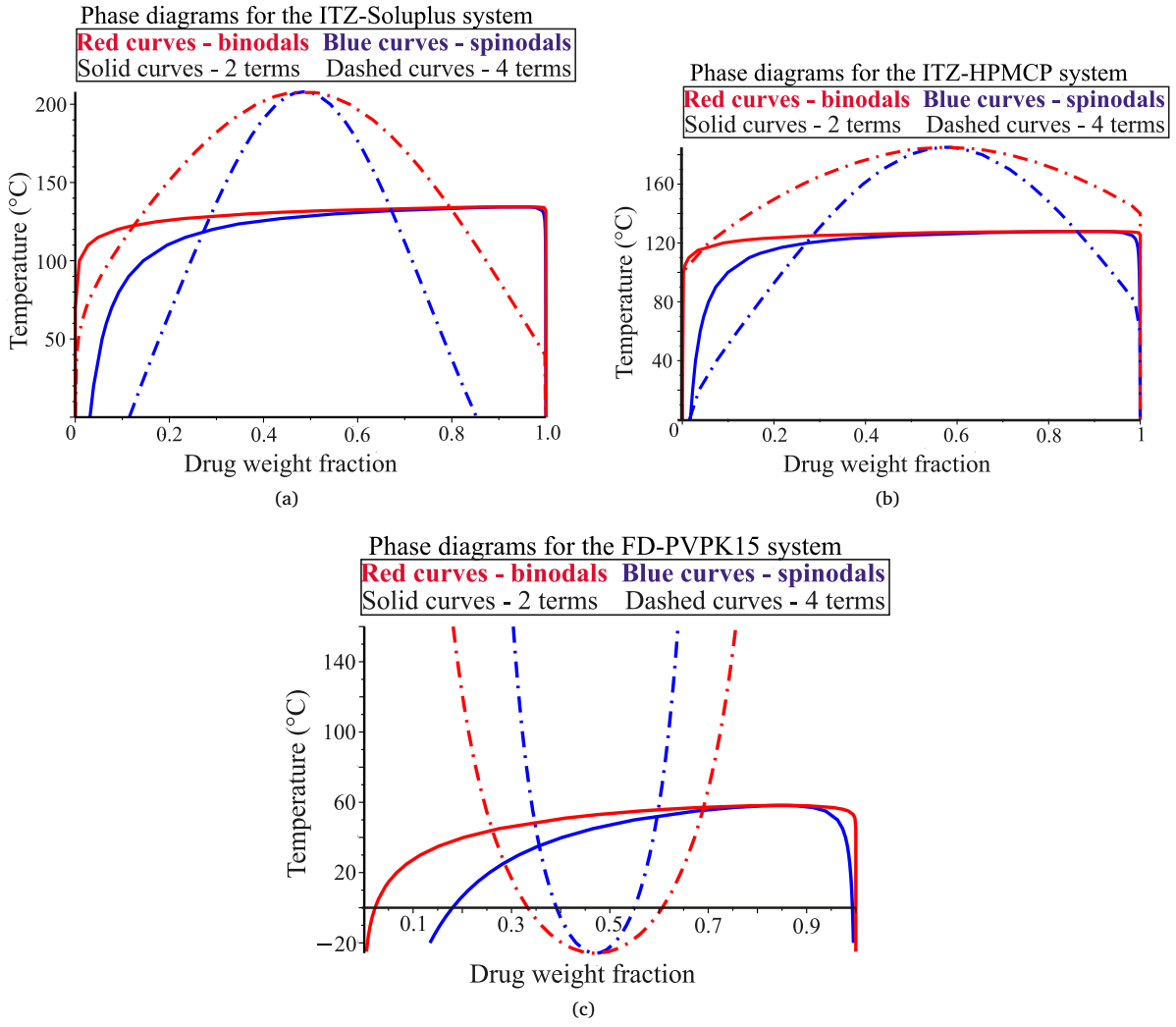

Fig. 1. Phase diagrams for three different binary solid dispersion systems. The phase diagrams are calculated based on FH interaction parameters taken from the literature. Each plot displays two sets of phase diagrams. One set (the solid lines) is calculated using a temperature-dependent interaction parameter $\chi_{dp} = \chi_{dp}(T)$. The other set (dashed-dotted lines) is calculated using a temperature- and composition-dependent interaction parameter $\chi_{dp} = \chi_{dp}(\phi_d, T)$. (a) ITZ-SOL system, with the interaction parameters taken from Potter et al. (2018). (b) ITZ-HPMCP system with the interaction parameters taken from Potter et al. (2018). (c) FD-PVPK15 system, with interaction parameters taken from Tian et al. (2013b) (temperature-dependent expression) and Tian et al. (2019) (temperature- and composition-dependent expression). See the main text for further discussion of this figure.

Table 3
Other parameter values for the three binary solid dispersions considered in this study. Here ρ is the mass density, M is the molecular mass, V is the molar volume.

System	ρ (g/cm^3)	M (g/mole)	V (cm^3/mole)	$m = V_p/V_d$
Itraconazole (ITZ)	1.27 (ChemicalBook Inc, 2025)	705.64	555.62	–
Felodipine (FD)	1.28	383.07	300.19 (Tian et al., 2013a)	–
Soluplus (SOL)	1.082 (BASF SE, 2025)	118 000	109 057	–
HPMCP	1.29 (Karandikar et al., 2015)	37 902	29 381	–
PVPK15	1.20 (Ataman Kimya A. S., 2025)	9000	7500	–
ITZ-SOL	–	–	–	196.28
ITZ-HPMCP	–	–	–	52.88
FD-PVPK15	–	–	–	24.98

phase diagrams are plotted in Fig. 1, where we display the spinodal and binodal curves for each of the three systems, and with drug weight fraction on the horizontal axis and temperature on the vertical axis. The intersections of the binodal and spinodal curves give the critical points. Each plot in the figure corresponds to a different system, and displays two sets of phase diagrams — one for a temperature-dependent FH parameter and one for a temperature- and composition-dependent parameter.

Inspecting the three plots in Fig. 1, it is immediately clear that the phase diagrams predicted by the two-term (temperature-dependent)

Table 4
Some key parameters for the plots in Fig. 1. Here T_c is the critical temperature, X_c is the critical drug concentration expressed as a molar fraction, W_c is the critical drug concentration expressed as a weight fraction, and τ is a parameter that determines the type of the critical point (UCST or LCST) - see Eqs. (18) and (19).

Form of χ_{dp}	Figure	T_c (°C)	X_c	W_c	τ
$\chi_{\mathrm{ITZ-SOL}}(T)$	Fig. 1(a)	134.43	0.9996	0.9427	14 658.93 > 0 (UCST)
$\chi_{\mathrm{ITZ-SOL}}(\phi_{\mathrm{ITZ}}, T)$	Fig. 1(a)	207.97	0.9937	0.4849	16 295.77 > 0 (UCST)
$\chi_{\mathrm{ITZ-HPMCP}}(T)$	Fig. 1(b)	127.87	0.9974	0.8774	305.57 > 0 (UCST)
$\chi_{\mathrm{ITZ-HPMCP}}(\phi_{\mathrm{ITZ}}, T)$	Fig. 1(b)	185.02	0.9864	0.5753	1169.16 > 0 (UCST)
$\chi_{\mathrm{FD-PVPK15}}(T)$	Fig. 1(c)	58.22	0.9921	0.8491	290.12 > 0 (UCST)
$\chi_{\mathrm{FD-PVPK15}}(\phi_{\mathrm{FD}}, T)$	Fig. 1(c)	−25.89	0.9518	0.4706	−887.56 < 0 (LCST)

interaction expressions differ significantly from the diagrams predicted by the corresponding four-term (temperature- and composition-dependent) expressions. The diagrams predicted by the four-term expressions *do not* correspond in any case to a minor refinement of the corresponding diagrams predicted by the two-term expressions; in all three cases they differ substantially. For the ITZ-SOL and ITZ-HPMCP systems, the four-term expressions predicted higher critical temperatures and lower critical drug concentrations — see Table 4. For the FD-PVPK15 system (Fig. 1(c)), the two sets of phase diagrams differ dramatically. Notably, the two-term expression predicts an upper critical solution temperature (UCST), whereas the four-term expression predicts a lower critical solution temperature (LCST), highlighting a significant inconsistency.

Nevertheless, for all three systems considered in Fig. 1, there are areas of overlap for the two sets of phase diagrams where their predictions for the system's stability agree. However, it should also be noted there are also significant regions where the two phase diagrams outright disagree in their stability predictions, particularly for the FD-PVPK15 system.

3.2. Experimental challenges and fitting procedures

In this section, we make a few brief remarks about some experimental challenges in the context of solid dispersions, and the fitting of experimental data to the functional forms (4) and (5). A summary of the experimental methods used to determine the FH interaction parameters used in this study can be found in Table 2.

3.2.1. Experimental challenges

When evaluating the stability of solid dispersions under typical storage conditions, the temperatures of interest typically lie in the range 15 °C to 30 °C. However, thermal methods such as the melting point depression method or the residual crystallinity method usually probe the behaviour of solid dispersions at temperatures that are much higher than this - temperatures of well over 100 °C are common. Furthermore, the temperature values obtained using thermal methods can frequently be relatively closely bunched together. Expressions for the FH interaction parameter based on such experiments can be of value for higher temperatures, but may be of limited utility for the lower temperatures typical of storage conditions. Nevertheless, higher temperatures can be of real practical relevance - for example, in the context of the hot melt extrusion process. A hot melt extrusion is a continuous manufacturing process in which a drug is molecularly dispersed in a molten polymer matrix under heat and shear to form a solid dispersion (Ghebre-Sellassie et al., 2018).

One method to evaluate the behaviour of solid dispersions at lower temperatures is to introduce a third component (water, for example) into the system to act as an accelerant for phase separation (Tian et al., 2019). The temperature at which the single glass transition temperature T_g of the solid dispersion separates into two distinct T_g values can then be used as an estimate for the binodal point, as assessed by differential scanning calorimetry. However, the underlying theoretical framework for ternary systems is considerably more complex than that for binary systems, and the corresponding experimental approach will necessarily be also more involved. Nevertheless, the FH values estimated in this manner may be used to develop FH interaction formulae that are more appropriate for storage conditions. Developing formulae that are valid across a broad range of temperature values would ideally involve experimental techniques spanning a similarly wide temperature range, with well-distributed temperature data points - a requirement that we appreciate may be difficult to achieve in practice. Well-distributed temperature data are particularly important for the reliable determination of the temperature dependence of the FH interaction parameter χ, as narrow temperature ranges lead to strong correlations between fitted coefficients and poorly constrained extrapolations to lower temperatures.

3.2.2. Fitting procedures

Expressions of the form (4) and (5) for FH interaction parameters are typically developed using experimental data points and a least-squares fitting procedure - see Table 2. Once a fitting has been completed, it is of value to critically evaluate the quality of the fitting using a *sensitivity analysis*. A sensitivity analysis involves assessing the effect that relatively small changes in the experimental data points can have on the values of the fitting parameters. We evaluated the sensitivity of one of the fitting procedures described in Table 2 using the `numpy.linalg.lstsq` routine from the NumPy library (Harris et al., 2020).

In Appendix C, we considered the stability of the least-squares fitting procedure for the FD-PVPK15 system, as developed in Tian et al. (2019). In this appendix, we display some illustrative calculations that demonstrate the sensitivity of the results to the values of experimental data points. It was shown that a relatively small change in the value of just one experimental data point can lead to a dramatic change in the values of the fitting parameters. In one example, it was shown that changing just one of the data points by 5% can lead to an over 80% change in one of the fitted parameters, indicating an unstable fitting procedure.

Several approaches may be adopted to mitigate instability in a fitting procedure of the kind just described. As previously alluded to, one obvious (and perhaps practically unhelpful) suggestion is to perform more experimental measurements, and to distribute them over a broader temperature range. It can also be of value to monitor the condition number of the design matrix of the least-squares fitting - a large condition number is indicative of ill-conditioning; see Chapter 4 of the book (Sauer, 2012), for example. It may also be worth designing a more robust fitting model by using a more sophisticated procedure. One possibility here is ridge regression, as described in Chapter 3 of the book (Hastie et al., 2009).

3.3. Evolution of the FD-PVPK15 system

In Fig. 2, we plot two phase diagrams for the FD-PVPK15 system — one diagram based on the two-term expression for $\chi = \chi(T)$ (Fig. 2(a)), and the other based on the four-term expression for $\chi = \chi(\phi_d, T)$ (Fig. 2(b)). On both of these diagrams, we superimpose numerical solutions to the corresponding partial differential equation in a two-dimensional square domain (see Section 2.2). The non-dimensional

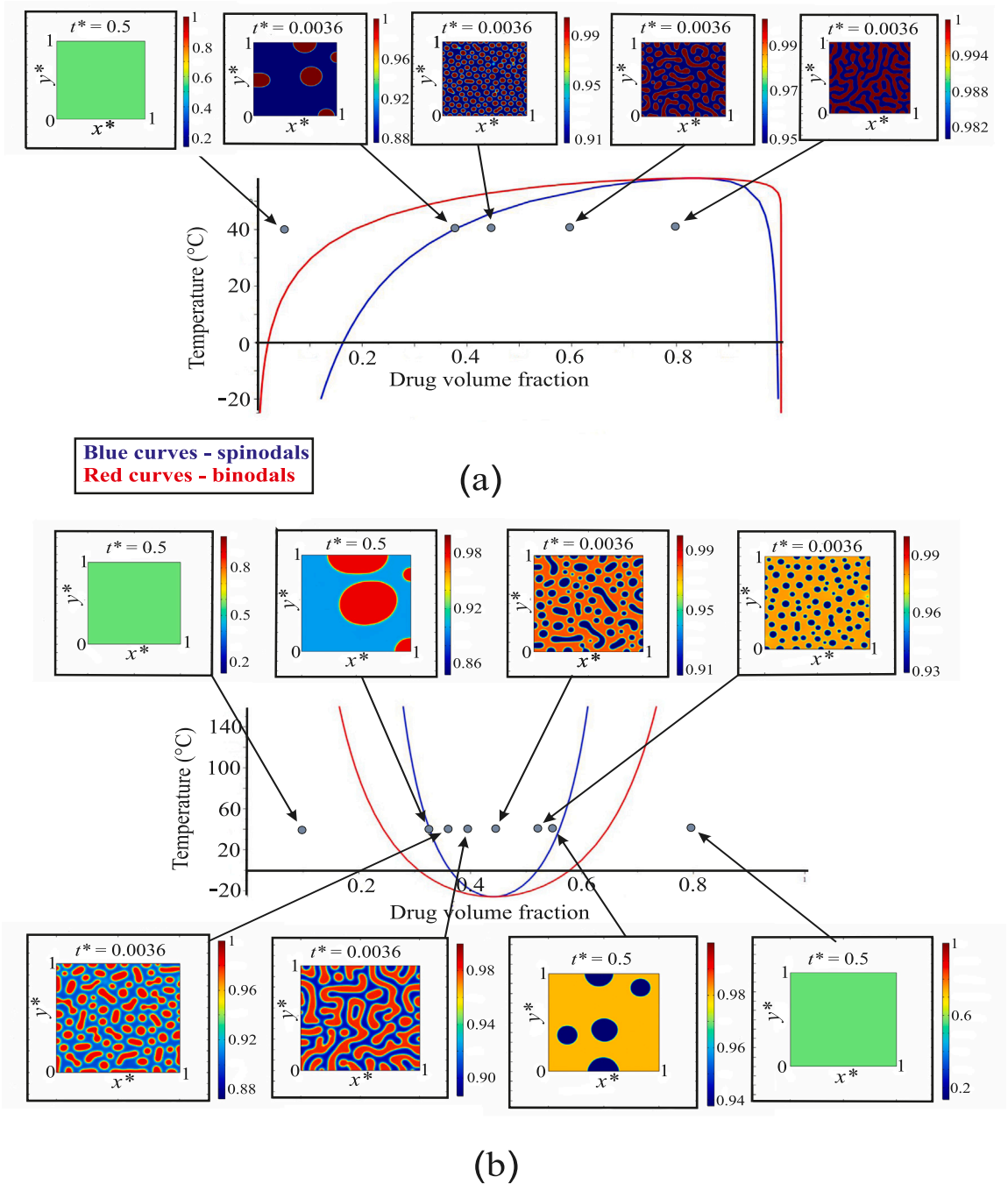

Fig. 2. Numerical solutions superimposed on a phase diagrams for the FD-PVPK15 system. Here (a) displays a phase diagram correspoinding to a temperature-dependent interaction parameter $\chi_{dp} = \chi_{dp}(T)$, and (b) displays a phase diagram corresponding to a temperature- and composition-dependent interaction parameter $\chi_{dp} = \chi_{dp}(\phi_d, T)$. The parameter values used can be found in Section 2.3.3. The blue regions are polymer-enriched and the red regions are drug-enriched. The green panels correspond to cases where phase separation does not occur.

time t^* is displayed on each solution panel in the diagram. Each of the solution panels has an arrow pointing to the location in the phase diagram for the mean value of the initial condition for the drug volume fraction ϕ_d. The colour bars on each solution panel refer to the molar fraction of drug. When a system phase separates, it splits into two co-existing phases determined by the two binodal points for that temperature. The left point is polymer-enriched (bluer regions), and the right point is drug enriched (redder regions). Notice that most of the solution panels displayed primarily consist of just two distinct colours, corresponding to these two phases. All of the solution panels displayed here correspond to a temperature of 40 °C.

In Fig. 2(a), the critical value for the composition is $\phi_{dc} \approx 0.8333$ and for $T = 40\,°\text{C}$, the left and right binodal points are $\phi_{dL} \approx 0.1840$ and $\phi_{dR} \approx 1$, respectively. The solution panel that has its average initial drug volume fraction closest to ϕ_{dc} (the one furthest to the right) has a bicontinuous network with a labyrinthine structure, as would be expected for initial compositions close to the critical composition ϕ_{dc}; for an explanation of this, see, for example, the review article by Bray (1994). As the composition shifts to the left of ϕ_{dc}, the panels

show drug droplets embedded in a polymer-rich phase, and this is again in line with expectations here (see Bray (1994)). The solution panel corresponding to the point to the left of ϕ_{dL} is uniformly green, indicating the absence of phase separation, in agreement with the theoretical prediction.

Fig. 2(b) shows the phase diagram based on the four-term (composition-dependent) FH interaction parameter. For this case, the critical value for the composition is $\phi_{dc} \approx 0.4412$, and for $T = 40\,^{\circ}\mathrm{C}$ the left and right binodal points are $\phi_{dL} \approx 0.2435$ and $\phi_{dR} \approx 0.6457$, respectively. Similar remarks to those for part (a) above apply here, with the behaviour again following expectations — note in particular the string-like behaviour close to $\phi_d = \phi_{dc}$ and the formation of droplets closer to the metastable regions.

4. Conclusions

This work establishes a rigorous, composition-dependent FH mathematical framework for phase-diagram construction and stability analysis in polymer–solute systems, applied to pharmaceutical solid dispersions. We derived expressions for the chemical potentials and associated stability conditions in the case $\chi = \chi(\phi, T)$, and used these to construct phase diagrams, enabling direct comparison for the corresponding cases where χ is treated as a function of temperature alone. Within this formulation we obtained generalized criteria for the presence of UCST and LCST type behaviour, demonstrating explicitly how the composition dependence of χ modifies the underlying thermodynamic structure. Across three representative systems, we showed that $\chi = \chi(\phi, T)$ and $\chi(T)$ models can yield markedly different predictions, not only shifting coexistence boundaries but, in some cases, changing qualitative conclusions about phase behaviour and stability. In particular, composition dependence can alter the extent and topology of metastable and unstable regions and can even reverse the predicted UCST/LCST character, thereby changing the inferred mechanism of demixing. These differences translate directly into distinct formulation and storage implications when phase diagrams are used to guide stability decisions. To connect thermodynamic predictions to microstructural spatiotemporal evolution, we embedded the composition-dependent free energy into a Cahn–Hilliard type phase-field model. The resulting simulations demonstrate that changes in the stability landscape as a result of the different forms of χ lead to distinct demixing pathways and morphologies, consistent with the revised spinodal and binodal structure.

A key strength of the present formulation is its generality. Although the illustrative phase-diagram calculations employed a quadratic composition dependence for the FH interaction parameter, the framework itself places no restriction on the functional form of $\chi(\phi, T)$. The derived expressions for the chemical potentials, stability criteria and evolution equations therefore remain valid for arbitrary composition dependence, enabling straightforward incorporation of more sophisticated experimentally fitted or physically motivated interaction models (see, for example, Wolf (2003)).

Taken together, our results show that incorporating $\chi = \chi(\phi, T)$ may be necessary to obtain mechanistically faithful and decision-relevant phase-diagram predictions. More broadly, our results highlight the importance of careful parameter fitting and model selection, to ensure that experimental calibration data lead to thermodynamic models that remain predictive outside the fitted conditions. Overall, this work provides a rigorous and general thermodynamic–kinetic framework for incorporating $\chi(\phi, T)$ into FH phase-diagram construction, demonstrating that composition dependence can fundamentally change stability predictions and therefore the design and risk assessment of solid-dispersion products.

CRediT authorship contribution statement

Martin Meere: Writing – review & editing, Writing – original draft, Visualization, Software, Methodology, Investigation, Formal analysis, Conceptualization. **Giuseppe Pontrelli:** Writing – review & editing, Visualization, Software, Methodology, Investigation, Formal analysis, Conceptualization. **Sean McGinty:** Writing – review & editing, Resources, Methodology, Investigation, Funding acquisition, Formal analysis, Conceptualization.

Declaration of competing interest

The authors declare the following financial interests/personal relationships which may be considered as potential competing interests: Sean McGinty reports financial support was provided by Engineering and Physical Sciences Research Council. If there are other authors, they declare that they have no known competing financial interests or personal relationships that could have appeared to influence the work reported in this paper.

Appendix A. A PDE formulation in terms of an effective diffusion coefficient

The PDE governing the spatio-temporal evolution of the drug molar fraction $X_d = X_d(x, y, t)$ is given in the main text of the paper by (22). An equivalent formulation in terms of an effective diffusion coefficient $D_{\mathrm{eff}}(X_d)$ is given by (see Meere et al. (2019) for a derivation of this)

$$\frac{\partial X_d}{\partial t} = \nabla \cdot \left\{ D_{\mathrm{eff}}(X_d) \nabla X_d - D_d \delta_d^2 X_d \nabla \left(\nabla^2 X_d \right) \right\}, \tag{29}$$

where the effective concentration-dependent diffusion coefficient for the drug in the solid dispersion is

$$D_{\mathrm{eff}}(X_d) = D_{dd}(X_d) - V_d D_{dp}(X_d)/V_p = D_d \left\{ 1 + \frac{X_d}{\gamma_d} \left[\frac{\partial \gamma_d}{\partial X_d} - \frac{\partial \gamma_d}{\partial X_p} \right] \right\}, \tag{30}$$

and where γ_d is the activity coefficient of the drug — see Section 2.2. From (30) we then have (after some calculation)

$$\begin{aligned} D_{\mathrm{eff}}(\phi_d, T) = D_d(1 + (m-1)\phi_d) \big[1 + (1/m - 1)\,\phi_d + \\ \phi_d(1-\phi_d)\{-2\chi_{dp}(\phi_d, T) + 2(1-2\phi_d)\chi'_{dp}(\phi_d, T) \\ + \phi_d(1-\phi_d)\chi''_{dp}(\phi_d, T)\} \big]. \end{aligned} \tag{31}$$

The formulation (29)–(31) is mathematically equivalent to the Cahn-Hilliard formulation (22)–(24) given in Section 2.2. The expression (31) is useful because it provides information into how the mobility of the drug in the dispersion depends on the length of the polymer chains (m), the dispersion composition (ϕ_d), and the character of the drug-polymer interaction (χ_{dp}).

Appendix B. Criterion to determine whether a critical point is an UCST or a LCST

In this appendix, we determine a criterion to determine whether a critical point is an Upper Critical Solution Temperature (UCST) or a Lower Critical Solution Temperature (LCST). We recall that we are considering a binary mixture, and that we are plotting the phase diagram in (X_d, T) space where X_d is the molar fraction of the drug and T is the temperature. The Gibbs free energy of mixing is denoted by $\Delta G_{mix}(X_d, T)$, and for a given temperature T, the spinodal points are determined by solving

$$\frac{\partial^2 \Delta G_{mix}}{\partial X_d^2}(X_d, T) = 0$$

for X_d. Solving this equation for different temperatures T yields the spinodal curve in (X_d, T) space, and we denote this curve by

$$T = T_s(X_d).$$

Introducing the notation

$$F(X_d, T) = \frac{\partial^2 \Delta G_{mix}}{\partial X_d^2}(X_d, T)$$

we clearly then have that

$$F(X_d, T_s(X_d)) = 0$$

since the points on the spinodal curve satisfy this equation. Then

$$\frac{d}{dX_d} F(X_d, T_s(X_d)) = \frac{\partial F}{\partial X_d}(X_d, T_s(X_d)) + \frac{\partial F}{\partial T}(X_d, T_s(X_d)) \frac{dT_s(X_d)}{dX_d} = 0 \tag{32}$$

so that

$$T_s'(X_d) = -\left(\frac{\frac{\partial F}{\partial X_d}}{\frac{\partial F}{\partial T}} \right)_{(X_d, T_s)} = -\left(\frac{\frac{\partial^3 \Delta G_{mix}}{\partial X_d^3}}{\frac{\partial^3 \Delta G_{mix}}{\partial X_d^2 \partial T}} \right)_{(X_d, T_s)}, \tag{33}$$

where here $T_s'(X_d) = dT_s(X_d)/dX_d$. We denote a critical point by $X_d = X_c$ and $T = T_c$. At a critical point we have

$$T_s'(X_c) = 0,$$

and so it follows from (33) that

$$\frac{\partial^3 \Delta G_{mix}}{\partial X_d^3}(X_c, T_c) = 0, \tag{34}$$

and since the critical point also lies on the spinodal curve, we have that

$$\frac{\partial^2 \Delta G_{mix}}{\partial X_d^2}(X_c, T_c) = 0. \tag{35}$$

Eqs. (34) and (35) give two equations to determine the two unknowns X_c and T_c (the critical point).

To determine if the critical point corresponds to a LCST or an UCST, we need to determine the curvature of the spinodal curve at the critical point, $T_s''(X_c)$. If the critical point $X_d = X_c$ is a LCST, then it corresponds to a local minimum of the spinodal curve, so that $T_s''(X_c) > 0$. If $X_d = X_c$ is an UCST, then it is a local maximum of the spinodal curve, so that $T_s''(X_c) < 0$. Taking the total derivative of (32) with respect to X_d leads to

$$\frac{\partial^2 F}{\partial X_d^2} + 2\frac{\partial^2 F}{\partial X_d \partial T} T_s'(X_d) + \frac{\partial F}{\partial T} T_s''(X_d) + \frac{\partial^2 F}{\partial T^2} \left(T_s'(X_d) \right)^2 = 0 \tag{36}$$

where in this expression the derivatives are evaluated at X_d and $T = T_s(X_d)$. Setting $X_d = X_c$ in (36) gives

$$T_s''(X_c) = -\left(\frac{\frac{\partial^2 F}{\partial X_d^2}}{\frac{\partial F}{\partial T}} \right)_{(X_c, T_c)} = -\left(\frac{\frac{\partial^4 \Delta G_{mix}}{\partial X_d^4}}{\frac{\partial^3 \Delta G_{mix}}{\partial X_d^2 \partial T}} \right)_{(X_c, T_c)}. \tag{37}$$

This gives the following criteria. If

$$\left(\frac{\frac{\partial^4 \Delta G_{mix}}{\partial X_d^4}}{\frac{\partial^3 \Delta G_{mix}}{\partial X_d^2 \partial T}} \right)_{(X_c, T_c)} < 0 \quad \Rightarrow \quad (X_c, T_c) \text{ is a LCST}, \tag{38}$$

and if

$$\left(\frac{\frac{\partial^4 \Delta G_{mix}}{\partial X_d^4}}{\frac{\partial^3 \Delta G_{mix}}{\partial X_d^2 \partial T}} \right)_{(X_c, T_c)} > 0 \quad \Rightarrow \quad (X_c, T_c) \text{ is an UCST}. \tag{39}$$

B.1. The criterion in terms of an effective diffusion coefficient

We now apply the criteria given by (38) and (39) to the case of a FH binary mixture with a composition dependent interaction parameter. Using the effective diffusion coefficient $D_{\text{eff}}(\phi_d, T)$ introduced in Appendix A, a straightforward calculation shows that for this case

$$T_s''(X_c) = -\left(\frac{\frac{\partial^2 D_{\text{eff}}}{\partial \phi_d^2} \left(\frac{\partial \phi_d}{\partial X_d} \right)^2}{\frac{\partial D_{\text{eff}}}{\partial T}} \right)_{(X_c, T_c)}, \tag{40}$$

and the criteria (38) and (39) become

$$\left(\frac{\frac{\partial^2 D_{\text{eff}}}{\partial \phi_d^2}}{\frac{\partial D_{\text{eff}}}{\partial T}} \right)_{(\phi_c, T_c)} < 0 \quad \Rightarrow \quad (\phi_c, T_c) \text{ is a LCST}, \tag{41}$$

and if

$$\left(\frac{\frac{\partial^2 D_{\text{eff}}}{\partial \phi_d^2}}{\frac{\partial D_{\text{eff}}}{\partial T}} \right)_{(\phi_c, T_c)} > 0 \quad \Rightarrow \quad (\phi_c, T_c) \text{ is an UCST}, \tag{42}$$

where here ϕ_c is the volume fraction of drug at the critical point.

Appendix C. Stability of least-squares fitting

We considered the stability of the fitting procedure for the FD-PVPK15 system, as developed in Tian et al. (2019). We briefly describe the procedure here and display some illustrative calculations that demonstrate the sensitivity of the results to the values of experimental data points. Writing $x = 1/T$ where T is measured in Kelvin, $y = \phi_d$, $f = \chi_{\text{FD-PVPK15}}$, the fitting model is

$$f(x, y) = A + Bx + Cy + Ey^2 \tag{43}$$

where A, B, C and E are the constants to be fitted. The fitting is implemented using the eight experimental data points (x_i, y_i, f_i), $1 \leq i \leq 8$, taken from Tian et al. (2019), and displayed in Table 5 here. In these data points, the experimentalist has good control over the values for y_i (drug volume fractions), but the values for x_i (and consequently f_i) are subject to experimental error. Fitting this data to (43) using the routine `numpy.linalg.lstsq` gives

$$A = 1.714, \quad B = -850.969, \quad C = 5.174, \quad E = -7.853,$$

in good agreement with the results of Tian et al. (2019). We now illustrate how sensitive these values can be to slight changes in experimental values using two examples. Suppose we change just one of the values in Table 5 - specifically, decrease the value of x_1 by 5% so that $x_1 = 0.002289$, leaving the remaining values the same. Repeating the fitting procedure now gives

$$A = 0.709, \quad B = -590.279, \quad C = 5.779, \quad E = -8.088,$$

and this represents the following percentage changes in the values

$$A : 58.65\%, \quad B : 30.63\%, \quad C : 11.69\%, \quad E : 3\%.$$

As another example, suppose we increase the value of x_4 by 5% so that $x_4 = 0.002558$, leaving the rest of the values unchanged. The fitting procedure now gives

$$A = 3.205, \quad B = -1435.272, \quad C = 6.595, \quad E = -9.506,$$

representing the following percentage changes in the values

$$A : 86.99\%, \quad B : 68.65\%, \quad C : 27.45\%, \quad E : 21.07\%.$$

Clearly then, a relatively small change in the value of just one experimental data point can lead to a dramatic change in the values of the fitting parameters, indicating an unstable fitting procedure.

Table 5
Data for the FD-PVPK15 system taken from Tian et al. (2019). Here $x = 1/T$, $y = \phi_d$, and $f = \chi_{\text{FD–PVVPK15}}$.

	x_i	y_i	f_i
$i = 1$	0.00241	0.949	−2.66
$i = 2$	0.002417	0.899	−1.84
$i = 3$	0.002425	0.848	−1.48
$i = 4$	0.002436	0.798	−1.40
$i = 5$	0.003011	0.346	0.0293
$i = 6$	0.003057	0.396	−0.0823
$i = 7$	0.003104	0.446	−0.219
$i = 8$	0.003124	0.496	−0.284

Data availability

All data supporting this study are provided within the main text and appendix.

References

Altamimi, M., Neau, S., 2016. Use of the Flory–Huggins theory to predict the solubility of nifedipine and sulfamethoxazole in the triblock, graft copolymer soluplus. Drug Dev. Ind. Pharm. 42 (3), 446–455.

Ataman Kimya A. S., 2025. Ataman kimya a.s. https://www.atamanchemicals.com/pvp-k-15_u25060/. (Accessed 12 May 2025).

BASF SE, 2025. Basf. https://virtualpharmaassistants.basf.com/s/product?recordId=01t2p00000AjDlJAAV. (Accessed 12 May 2025).

Bray, A.J., 1994. Theory of phase-ordering kinetics. Adv. Phys. 43 (3), 357–459.

Brough, C., Williams, R.O. 3rd, 2013. Amorphous solid dispersions and nano-crystal technologies for poorly water-soluble drug delivery. Int. J. Pharm. 453, 157–166.

ChemicalBook Inc, 2025. Chemicalbook - chemical search engine. https://www.chemicalbook.com. (Accessed 12 May 2025).

Chen, W., Wang, C., Wang, X., Wise, S.M., 2019. Positivity-preserving, energy stable numerical schemes for the Cahn–Hilliard equation with logarithmic potential. J. Comput. Phys.: X 3, 100031.

COMSOL AB, 2024. COMSOL Multiphysics. COMSOL AB, Stockholm, Sweden, https://www.comsol.com.

Dhirendra, K., Lewis, S., Udupa, N., Atin, K., 2009. Solid dispersions: a review. Pak. J. Pharm. Sci. 22 (2), 234–246.

Flory, P.J., 1942. Thermodynamics of high polymer solutions. J. Chem. Phys. 10, 51–61.

Ghebre-Sellassie, I., Martin, C.E., Zhang, F., DiNunzio, J. (Eds.), 2018. Pharmaceutical Extrusion Technology. In: Drugs and the Pharmaceutical Sciences, CRC Press, Taylor & Francis Group, Boca Raton, FL, USA.

Harris, C.R., Millman, K.J., van der Walt, S.J., Gommers, R., Virtanen, P., Cournapeau, D., Wieser, E., Taylor, J., Berg, S., Smith, N.J., et al., 2020. Array programming with NumPy. Nature 585 (7825), 357–362.

Hastie, T., Tibshirani, R., Friedman, J., 2009. The Elements of Statistical Learning: Data Mining, Inference, and Prediction, second ed. Springer.

Hiemenz, P.C., Lodge, T.P., 2007. Polymer Chemistry, second ed. CRC Press, Boca Raton, Florida.

Huang, Y., Dai, W., 2014. Fundamental aspects of solid dispersion technology for poorly soluble drugs. Acta Pharm. Sin. B 4 (1), 18–25.

Huggins, M.L., 1941. Solutions of long chain compounds. J. Chem. Phys. 9.

Karandikar, H., Ambardekar, R., Kelly, A., Gough, T., Paradkar, A., 2015. Systematic identification of thermal degradation products of HPMCP during hot melt extrusion process. Int. J. Pharm. 486 (1–2), 252–258.

Kim, D., Kim, Y., Tin, Y.-Y., Soe, M.-T. P., Ko, B., Park, S., Lee, J., 2021. Recent technologies for amorphization of poorly water-soluble drugs. Pharmaceutics 13 (8), 1318.

Klueppelberg, J., Handge, U.A., Thommes, M., Winck, J., 2023. Composition dependency of the Flory–Huggins interaction parameter in drug–polymer phase behavior. Pharmaceutics 15 (12).

Koningsveld, R., 1994. Thermodynamics of polymer blends. Macromol. Symp. 78 (1), 1–13.

Koningsveld, R., Solc, K., MacKnight, W.J., 1993. Thermodynamic aging of immiscible polymer blends. Macromolecules 26 (24), 6676–6678.

Meere, M., Pontrelli, G., McGinty, S., 2019. Modelling phase separation in amorphous solid dispersions. Acta Biomater. 94, 410–424.

Potter, C.B., Davis, M.T., Albadarin, A.B., Walker, G.M., 2018. Investigation of the dependence of the Flory–Huggins interaction parameter on temperature and composition in a drug–polymer system. Mol. Pharm. 15 (11), 5327–5335, PMID: 30259745.

Rask, M., Knopp, M., Olesen, N., Holm, R., Rades, T., 2018. Comparison of two DSC-based methods to predict drug-polymer solubility. Int. J. Pharm. 540 (1–2), 98–105.

Rumondor, A.C.F., Stanford, L.A., Taylor, L.S., 2009. Effects of polymer type and storage relative humidity on the kinetics of felodipine crystallization from amorphous solid dispersions. Pharm. Res. 26 (12), 2599–2606.

Sauer, T., 2012. Numerical Analysis, second ed. Pearson Education Limited, Harlow, England/Boston, MA.

Siepmann, J., Rades, T., Muellertz, A., Loftsson, T., 2020. Poorly soluble drugs. Int. J. Pharm. 577, 119055.

Taylor, D.M.L., 2018. The application of temperature-composition phase diagrams for hot melt extrusion processing of amorphous solid dispersions to prevent residual crystallinity. Int. J. Pharm. 553 (1–2), 454–466.

Tian, Y., Booth, J., Meehan, E., Jones, D., Li, S., Andrews, G., 2013a. Construction of drug-polymer thermodynamic phase diagram using Flory–Huggins interaction theory: identifying the relevance of temperature and drug weight fraction to phase separation within solid dispersions. Mol. Pharm. 10, 236–248.

Tian, Y., Caron, V., Jones, D.S., Healy, A.M., Andrews, G.P., 2013b. Using Flory–Huggins phase diagrams as a pre-formulation tool for the production of amorphous solid dispersions: a comparison between hot-melt extrusion and spray drying. J. Pharm. Pharmacol. 66, 256–274.

Tian, Y., Qian, K., Jacobs, E., Amstad, E., Jones, D.S., Stella, L., Andrews, G.P., 2019. The investigation of flory–huggins interaction parameters for amorphous solid dispersion across the entire temperature and composition range. Pharmaceutics 11 (8).

Tompa, H., 1956. Polymer Solutions, first ed. Butterworth scientific publications, London.

Wolf, B.A., 2003. Chain connectivity and conformational variability of polymers: Clues to an adequate thermodynamic description of their solutions ii: Composition dependence of Flory–Huggins interaction parameters. Macromol. Chem. Phys. 204 (11), 1381–1390.